A Multi-Phase Model for Plumes in Powder Injection Refining Processes

L. R. FARIAS and G. A. IRONS

A one-dimensional steady-state model for momentum transfer in ascending gas-liquid-powder plumes has been developed for conditions relevant to powder injection refining processes. Inter-phase transport of momentum permits the calculation of the volume fraction and velocity of the gas, liquid, and solid phases as they rise in the melt. The effects of plume geometry, initial conditions, density of the phases, head of liquid, bubble size, and powder loading and properties are assessed. Liquid velocities in gas-only injection into water compare favorably with available experimental data. Significantly lower liquid velocities are predicted in liquid metals. At solids loadings used in commercial powder injection stations, the powder is expected to have only a small effect on liquid velocity. For wire injection conditions with little gas release, liquid velocities are considerably smaller.

I. INTRODUCTION

In recent years the submerged injection of powders has gained importance as a means to carry out smelting and refining reactions because of the intimate contact between the fine particles and the metal. Familiar examples include the Mitsubishi Copper Smelting Process, the desulfurization of blast furnace iron with calcium carbide or mixtures of lime and magnesium, the desiliconization and dephosphorization of iron with iron oxide mixtures, and the calcium treatment of steel for desulfurization and sulfide shape control.

In spite of the importance of these types of reaction, the details of the particle trajectories, velocities, heating rates, and reaction rates are unknown. Work by the present authors has elucidated the states of flow in the conveying lines[1] and the implications for the regimes of flow in the descending or jet portion of the injection process.[2]

The present work is concerned with the ascending or plume region of the injection process. There have been several plume models proposed for ladles agitated by gas alone. Generally the aim of these models has been the prediction of the recirculating flow patterns or mixing time, and hence the treatment of the two-phase region has been simplified. They have all used mixture models which use volume-averaged velocities and densities, and thereby the two-phase region has been treated as a single phase. The constitutive relation between void fraction and velocity has either come from Wallis' Drift-Flux Model[3] for gas-water flow in a rigid vertical pipe,[4,5] an analysis of the slip between bubbles and liquid in a plume[6] or by solving the single phase flow equations allowing for diffusion of liquid.[7]

The disadvantage of such mixture models is that the discreteness of each phase is ignored, and average velocity, void fraction, and temperature are assigned to a particular point. Therefore the transport of momentum, heat, and mass between phases cannot be addressed by such models. It is only by formulating equations of continuity, momentum, and energy for each phase which include the interphase transport terms (for example, in the form of drag, heat transfer, and mass transfer coefficients) that one can calculate the changes in void fractions, velocities, temperatures, and compositions throughout the plume. In the present work, this approach is adopted for the calculation of phase velocity and volume fraction from the continuity and momentum equations. Among other aspects, this allows the investigation of the effects of changes in injection rates, liquid head, and bubble size. In addition the effects of powder addition can be assessed by simply including extra equations for this phase.

The present model is one-dimensional and steady-state which is thought to be a useful approximation. For vertical lancing, the predominant direction of motion is vertical, and therefore a model operating in this direction can yield average velocities and volume fractions of the phases during rise. For many engineering studies where liquid recirculation rate or average particle residence times are required, the radial distribution of these quantities is only of secondary interest.

II. OUTLINE OF THE MODEL

The physical situation of a downward injected jet is shown in Figure 1. On exit from the lance, the gas and powder flow together in a penetrating jet, entraining a small amount of liquid. The jet is slowed down by buoyancy forces and liquid entrainment until it reaches a maximum penetration where the velocity is zero. Predictions for the maximum jet penetration are available elsewhere.[2]

At this point gas and powder separate, and the gas forms large spherical cap bubbles (5 to 10 cm in diameter). The powder may remain inside the bubbles or outside in the liquid depending on the system. The gas and powder experience a force upward due to buoyancy and a force downward due to drag. Once these forces are in equilibrium, the gas and powder are expected to rise at a constant velocity relative to the liquid, but there will be a region in which the gas and particles are accelerating to their terminal velocities. The liquid experiences a force that is equal but opposite to the drag force on the gas and particles. Therefore, the liquid is accelerated, and will move with the gas and particles.

L. R. FARIAS, formerly with McMaster University, is Research Metallurgist with HyL Research and Development Center, Monterrey, N.L., Mexico. G. A. IRONS is Associate Professor, Department of Materials Science and Engineering, McMaster University, Hamilton, ON L8S 4L7, Canada.

Manuscript submitted November 29, 1984.

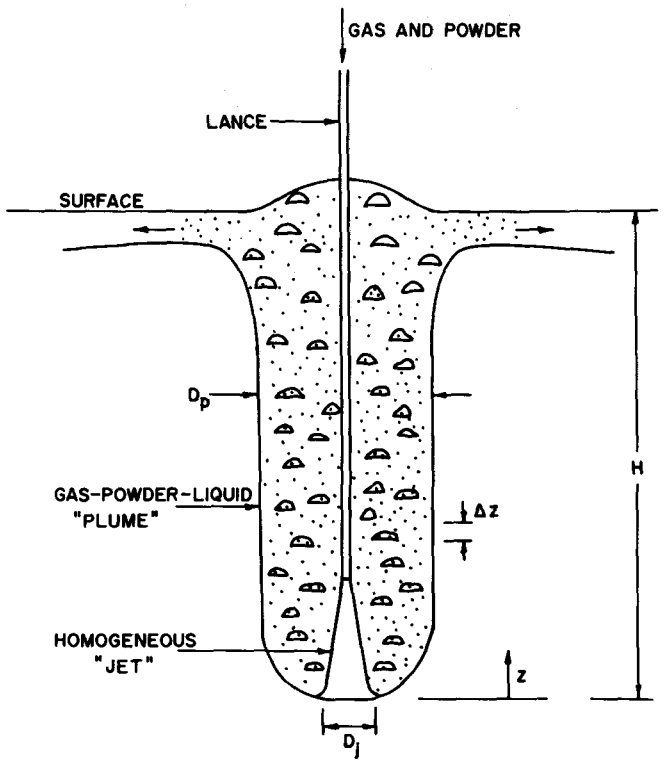

Fig. 1—Jet and plume concept.

Thereby, the liquid is entrained into the rising plume. Separate momentum equations must be written for the three phases given the large difference in phase velocity; for example, the gas bubble velocity is expected to be approximately 0.5 m per second greater than liquid velocity.

The principal assumptions used in this steady-state isothermal model are:

(a) The flow is one-dimensional, along the axis of the plume.
(b) All variables and properties are averaged across the plume diameter.
(c) The plume diameter is known from experiment.
(d) The area of the lance is ignored.
(e) Momentum is not changed by viscosity, turbulence, surface wave production, or other forces except buoyancy.
(f) Particles and gas reaching the surface are lost from the system.
(g) Liquid entrainment into the plume is governed by drag forces only.
(h) Gas and particle concentrations are low enough that single particle drag coefficients can be used, and that bubble-bubble and particle-particle interactions can be ignored.
(i) The partition of particles between the liquid and gas is considered an independent variable.
(j) The ladle is large enough that the pressure outside the plume is given by the head of liquid.
(k) The gas is at the liquid temperature.
(l) The bubble size is known and considered to be constant during rise.
(m) At the deepest point of penetration, which is the starting point for these calculations, the three phases are assumed to have a rising velocity that is much smaller than the terminal velocities.
(n) Added mass and history terms[8] are superfluous when the cross-sectional averaged momenta of all phases are considered.

In steady state, conservation of mass of gas-powder mixture in the bubbles indicates

$$\frac{d(\rho_m U_g A_p)}{dZ} = 0 \qquad [1]$$

where

$$\rho_m = \theta_g \rho_g + f\theta_p \rho_p \qquad [2]$$

is the mass of gas and powder inside the bubbles per unit volume of (gas-powder-liquid) mixture. Similarly, for the powder in the liquid

$$\frac{d(1-f)\theta_p \rho_p U_p A_p}{dZ} = 0 \qquad [3]$$

The momentum balance on each phase in each unit volume of the plume can be written with functions for the buoyancy and drag forces operating on each phase

$$\frac{d\rho_m U_g^2 A_p}{dZ} = F_{gp}^B - F_{gp-l}^D \qquad [4]$$

$$\frac{d(1-f)\theta_p \rho_p U_p^2 A_p}{dZ} = F_p^B - F_{p-l}^D \qquad [5]$$

$$\frac{d\theta_l \rho_l U_l^2 A_p}{dZ} = F_{gp-l}^D + F_{p-l}^D \qquad [6]$$

The buoyancy forces for the gas and powder in the bubbles and the powder in the liquid, respectively, are:

$$F_{gp}^B = [\rho_l(\theta_g + f\theta_p) - \rho_m] g A_p \qquad [7]$$

and

$$F_p^B = (1-f)(\rho_l - \rho_p)\theta_p g A_p \qquad [8]$$

The interphase drag functions were developed as the product of the drag force on one particle or bubble and the number of particles or bubbles per unit volume of plume. For the gas and powder in the bubble it was assumed that the powder merely changed the apparent density of the bubble, not the nature of the boundary layer in which case the drag function is

$$F_{gp-l}^D = \frac{0.75\rho_l C_{Dg}(U_g - U_l)^2(\theta_g + f\theta_p)A_p}{d_b} \qquad [9]$$

Similarly for the particles rising in the liquid

$$F_{p-l}^D = \frac{0.75\rho_l C_{Dp}(U_p - U_l)^2(1-f)\theta_p A_p}{d_p} \qquad [10]$$

The gas density is a function of temperature and pressure

$$\rho_g = \frac{P_{atm} + \rho_l g(H - Z)}{RT_g} \qquad [11]$$

The bubble size is assumed to be constant during rise, that is, independent of gas pressure or temperature. It is postulated that bubbles reach a maximum stable bubble size that

is determined by the level of turbulence and the properties of the liquid. Since the mass of gas is conserved, the number of bubbles in a unit volume increases, and this is reflected in an increase in θ_g.

With regard to the initial conditions, previous work indicated that the liquid volume fraction is not very high at the bottom of the jet.[2] Therefore:

$$\theta_l = 0.1 \quad [12]$$

was chosen arbitrarily. It is subsequently shown that the results are very insensitive to the choice of θ_l. The gas powder volume fractions are then found

$$\theta_g = \theta_g^\circ - \theta_l \theta_g^\circ \quad [13]$$

and

$$\theta_p = \theta_p^\circ - \theta_l \theta_p^\circ \quad [14]$$

where θ_p° and θ_g° are the particle and gas fractions at the lance tip which are known from the injection conditions.

The gas and powder velocity can then be obtained, as

$$U_g = \frac{m_g + f m_p}{\rho_m A_p} \quad [15]$$

and

$$U_p = \frac{m_p}{\theta_p \rho_p A_p} \quad [16]$$

The area of the plume at $Z = 0$ is taken as the area of the descending jet when its momentum is completely dissipated. The cone angle of the descending jet in water-powder and lead-powder mixtures was experimentally determined to be approximately 5 deg.[2]

The liquid velocity at $Z = 0$ is unknown, but a good estimation can be obtained by using the average recirculation velocity. Here, the relation of Sano and Mori[4] is chosen.

$$U_l = U_{rc} = \frac{1.17(Q_{gm} g H A_p^2)^{0.339}}{\frac{\pi}{4}(D_L^2 - D_p^2)} \quad [17]$$

where Q_{gm} is the gas flow rate at the bulk liquid temperature and mean pressure.

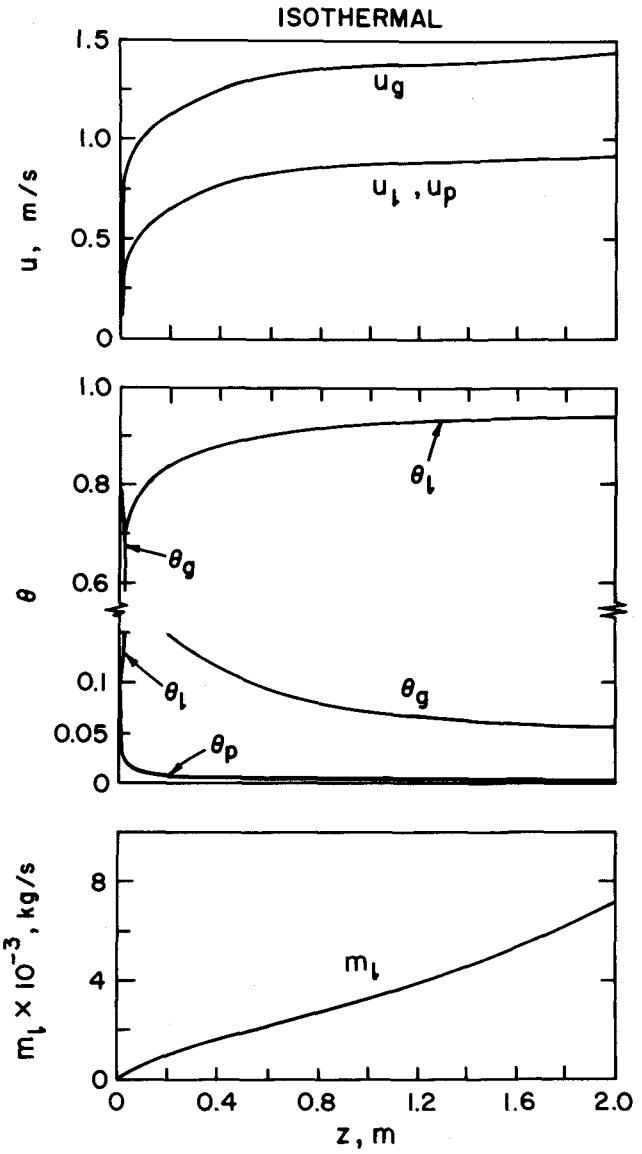

Fig. 2—Model results for isothermal injection of N_2-CaC_2 in 150 tonne iron ladle. m_g = 0.02 kg/s, m_p = 2.5 kg/s, f = 0, H = 2 m, D_L = 3.56 m, D_j = 0.5 m, α = 20 deg, d_b = 0.05 m, T_g (Z = 0) = 1673 K, T_{lb} = 1673 K.

III. RESULTS

Equations 1 through 6 were solved using Gear's[9] method for a system of stiff linear differential equations. Results were obtained for U_g, U_p, U_l, θ_g, θ_p as a function of input parameters m_g, m_p, plume geometry, bubble and particle size, fraction of powder in gas, and gas, powder, and liquid properties.

The entrained mass flow rate of liquid was obtained as

$$m_l = \theta_l \rho_l U_l A_p \quad [18]$$

Typical results of a calculation are shown in Figure 2, which simulates the injection of calcium carbide into a 150 tonne torpedo car. In this case it was assumed that the carrier gas instantaneously reached the metal temperature, 1400 °C, and there was no $CaCO_3$ added for gas release. One can see that velocities of all three phases quickly rise to velocities of the order of 1 m per second because of the nature of the equations as discussed below. Thereafter the velocities rise more slowly, principally due to the decreasing ferrostatic head, also discussed below. Even though the carbide is injected in the so-called dense phase regime, the volume fraction of solids in the plume is only about 0.003. It declines slowly during rise because the powder is distributed over a wider plume. The liquid fraction increases dramatically because the strong buoyancy forces acting on the gas also must drag the liquid with it, according to the coupling of the liquid and gas phases of Eqs. [4] and [6]. This liquid is entrained into the plume. The gas fraction decreases because it is spread over the wider plume cross-section and because the gas has been accelerated. In general, the average volume fractions of gas and powder were below 0.1 and 0.05, respectively, which supports the assumption that they act as single bubbles and particles.

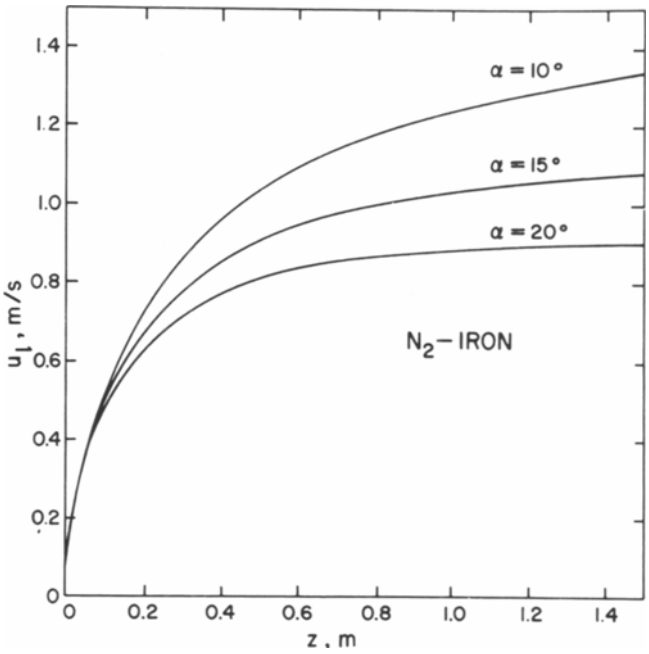

Fig. 3—Change in liquid velocity with height for conical plumes. N_2-iron system, m_g = 0.01 kg/s, H = 1.5 m, D_L = 2.2 m, D_j = 0.2 m, d_b = 0.05 m.

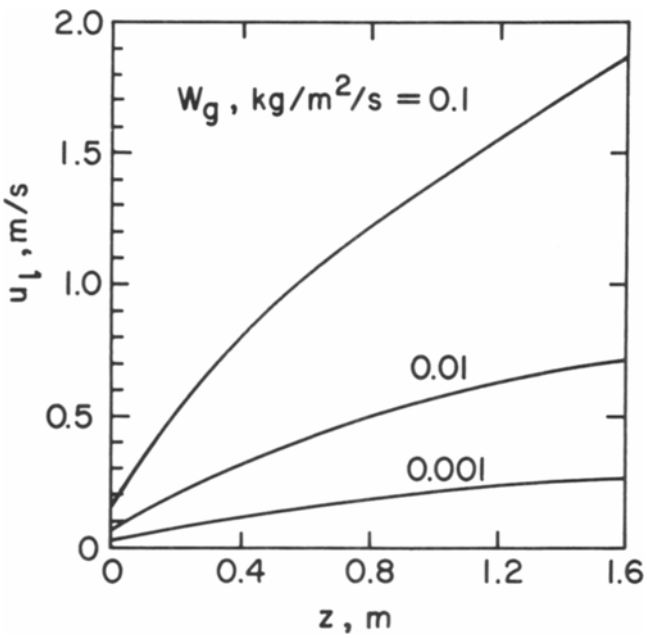

Fig. 5—Change in liquid velocity with height for a cylindrical plume. N_2-iron system, H = 1.5 m, D_L = 2.2 m, d_b = 0.05 m.

A. *Effect of Plume Geometry*

The liquid velocity for a conical plume in the N_2-iron system has been plotted as a function of Z in Figure 3. In this case there is no powder being injected, only gas. One sees that the liquid velocity rises from the average recirculation velocity of about 0.1 m per second to a significantly higher velocity, depending on the cone angle. If the bath were deep enough, the velocity would reach a maximum and then start dropping gradually.

There is controversy about the plume geometry. Hsiao *et al.*[10] and Szekely *et al.*[11] have proposed conical shapes for which the results in Figure 3 would apply. However, work by Fruehan and Martonik[12] suggests that the plume shape becomes cylindrical very quickly above the injection point. The plume initial geometry must be a function of the injection conditions of flow rate and nozzle orientation. No information was available for plumes developing from downward injection lances so an experiment was carried out to simulate this. Figure 4 shows the results of injection of nitrogen and Q-cel (inorganic microspheres, ρ_p = 240 kg/m^3, d_p = 70 μm) into water in a jetting regime. The ensuing rising plume is seen to be roughly cylindrical; this would appear to coincide with Fruehan and Martonik's observations. Further work is required to find plume shapes in liquid metals where the situation is far more complex than water, and indeed mercury models. Liquid velocity is shown for cylindrical plumes in Figure 5. Since the area of the plume is constant, it is useful to interpret the results in terms of the mass velocity of phase.

$$W_{\text{phase}} = \frac{m_{\text{phase}}}{A_p} \qquad [19]$$

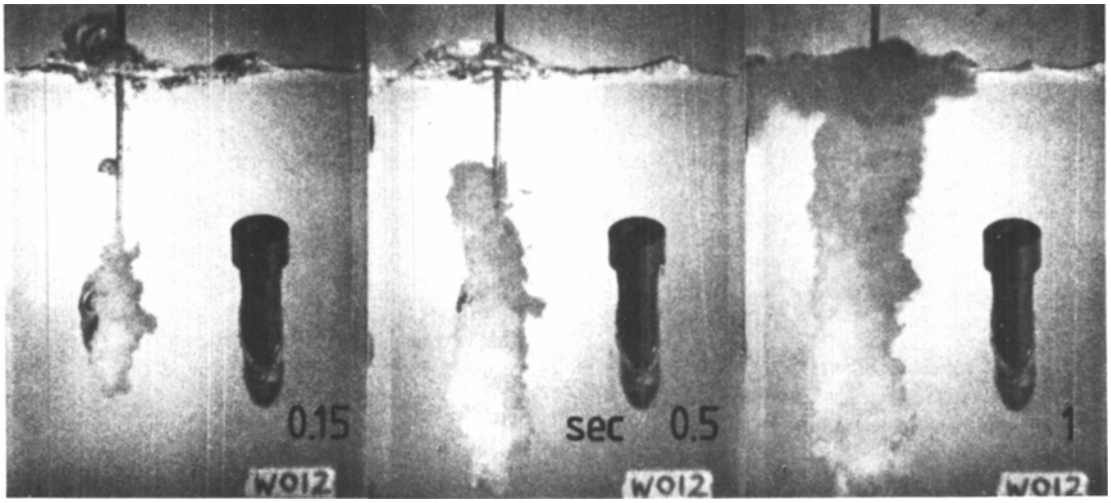

Fig. 4—Early stages of plume development in downward injection of N_2-Q-cel into water. m_p = 0.02 kg/s, m_g = 5.5 × 10^{-4} kg/s. Reduction by 6×.

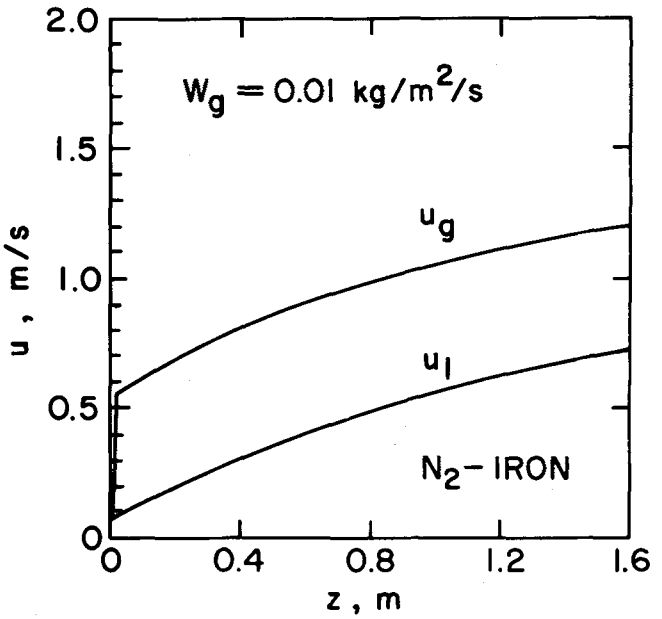

Fig. 6—Gas and liquid velocities for a cylindrical plume. N_2-iron system, W_g = 0.01 kg/m^2/s, H = 1.5 m, D_L = 2.2 m, d_b = 0.05 m.

The area of the plume can then be conveniently taken to be the breakthrough zone observed on the bath surface. In the rest of this paper cylindrical plumes will be assumed except where otherwise indicated.

B. *Effect of Initial Conditions*

The set of equations under consideration is made very stiff by the choice of initial conditions. Low density gas is placed at near zero velocity in a high density liquid. The resulting forces accelerate the gas to its terminal velocity in a very short distance. The drag force accelerates liquid in proportion to the square of the slip between gas and liquid and the ratio of the concentration of gas to liquid. A typical solution is shown in Figure 6 for a cylindrical plume. It was found that the initial conditions of phase concentration and velocity could be changed quite dramatically without any appreciable difference in the end results. However, when the initial gas velocity was set too high (comparable to U_T), the predicted velocities turned out larger. Normally, the gas initial velocities are expected to be about 1 cm per second. Typical starting conditions are shown in Table I. Thus it seems reasonable that the highly unstable conditions chosen for the initial conditions should quickly rearrange themselves to bubbles rising through the melt with a terminal velocity with respect to the liquid. The fact that at the start (Z = 0) bubbles can not exist when θ_g is 0.9 should not influence the final result once θ_g drops to lower values. Velocity solutions were also very insensitive to the choice of U_l at Z = 0. It was decided that the best estimation for U_l was the average recirculation velocity.

C. *Effect of Liquid Head*

The effect of variations in the height of the liquid head and the density of the liquid can be studied separately from the effects of thermal expansion with the aid of the model. In Figure 7, the liquid velocity is plotted as a function of height for liquids of different density corresponding to water, liquid iron, liquid copper, and liquid mercury, all hypothetically at room temperature with the same cone angle and initial bubble size. In this case, a conical plume with a 10 deg cone angle was chosen for the sake of comparison with aqueous results. One can see that for water the liquid velocity reaches a maximum velocity very quickly, and drops slowly thereafter because of the greater plume cross section. In contrast to this, the denser liquids exhibit lower liquid velocities due to the higher gas density but the velocity is ever increasing. This is due to the greater rate of volume expansion of the bubbles in dense liquids during rise, which produces more bubbles (according to the present assumptions). The greater number of bubbles creates more drag on the liquid. An alternate assumption, that the bubbles simply increase in volume, would have yielded a similar, but smaller effect. It should also be noted that the plume cone angles and initial bubble sizes are probably not the same for all liquid-gas combinations as assumed in this hypothetical case. However, these results suggest that water models should be used cautiously.

Table I. Typical Initial Conditions

$U_g = 0.7 \times 10^{-2}$ m/s	$\theta_g = 0.73$
$U_p = 0.12 \times 10^{-1}$ m/s	$\theta_p = 0.17$
$U_l = 0.73 \times 10^{-1}$ m/s	$\theta_l = 0.10$

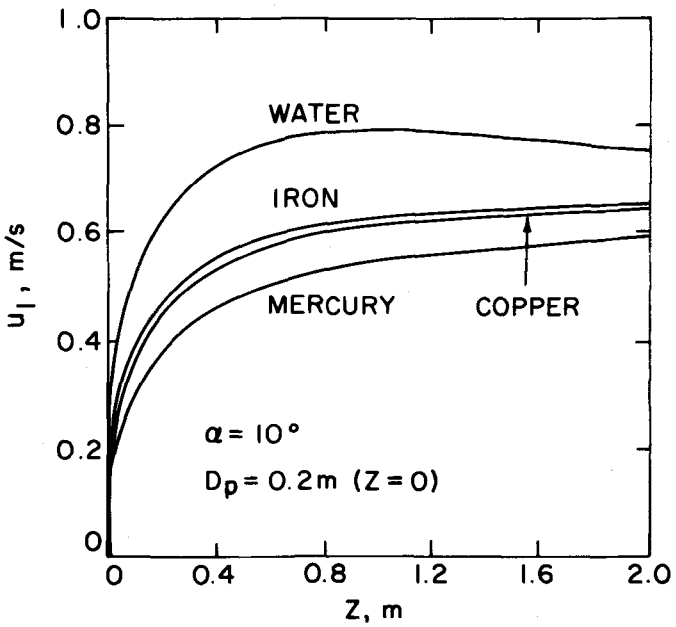

Fig. 7—Model results for hypothetical comparison between liquids of different densities with conical plumes. m_g = 0.01 kg/s, H = 2 m, D_L = 2 m, d_b = 0.05 m, $T_{lb} = T_g$ = 298 K.

D. *Effect of Bubble Size*

The bubble size in the plume is unknown; however, it must depend on liquid properties and gas flow rate. The effect that the powder would have on bubble size is also unknown. Estimations can be made from the experimental results of Sano and Mori;[13] for the iron system the bubble

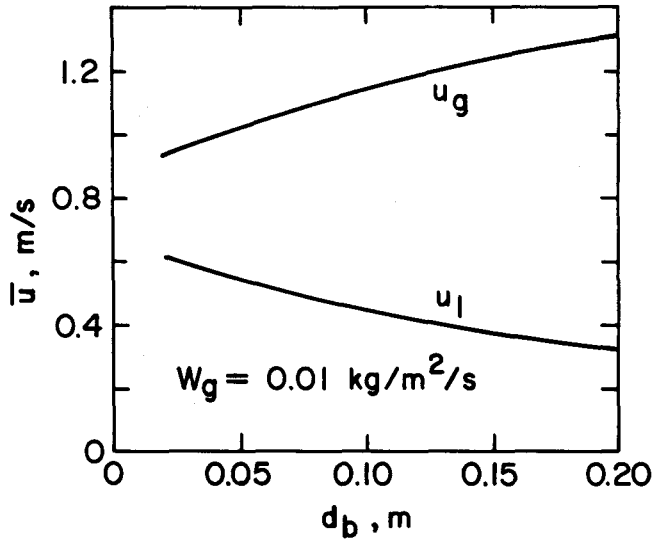

Fig. 8—Average gas liquid velocities as a function of bubble size. N_2-iron system, W_g = 0.01 kg/m^2/s, $H = D_L$ = 3.56 m.

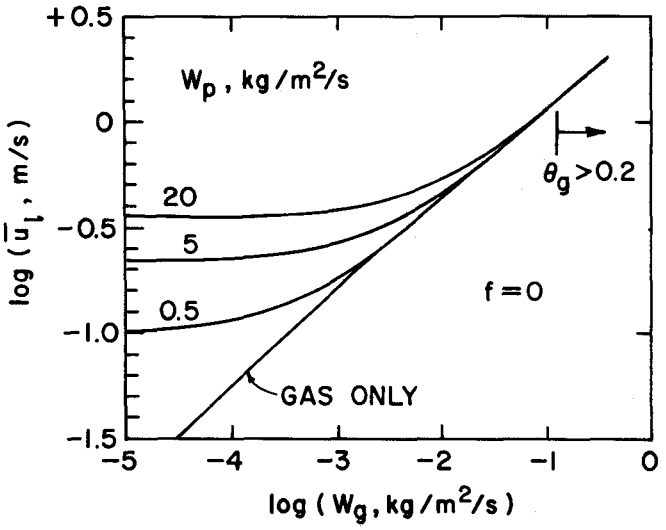

Fig. 9—Average liquid velocity as a function of mass velocity of gas and powder. N_2-CaC_2-iron system, d_b = 0.05 m, d_p = 100 μm, H = 1.5 m, D_L = 2.2 m.

diameter is likely to be between 2 and 10 cm. These large bubbles are of spherical cap shape and their drag coefficient is 8/3, when they rise in inviscid liquids. Figure 8 shows the influence of the bubble size on liquid velocity for a given mass velocity of gas. Here, the average liquid velocity is plotted

$$\overline{U}_l = \frac{1}{H} \sum_{Z=0}^{Z=H} U_l \Delta z \qquad [20]$$

Smaller bubbles exert a larger force on the liquid than large ones. This is because there are more small bubbles in the plume than large ones for a given gas flow rate. In consequence, the liquid accelerates to a higher velocity. The gas velocity, however, increases with bubble size because the terminal velocity increases. It can be seen that the changes in gas velocity are relatively insensitive to bubble size; from 2 cm to 10 cm diameter, U_l drops only 25 pct. Given that there are no data on bubble sizes in gas-powder plumes in iron baths, a middle of the range bubble size of 5 cm was chosen to generate results.

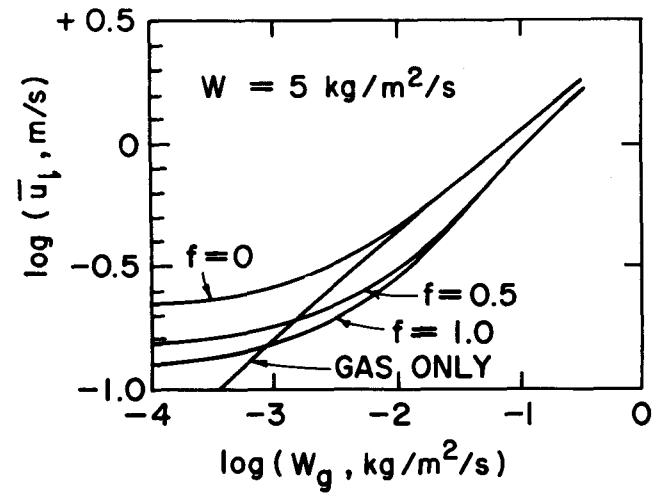

Fig. 10—Average liquid velocity as a function of mass velocity of gas for various powder in gas fractions. Conditions as in Fig. 9.

E. *Effect of Powder*

When powder is injected along with the gas it can be expected that since it is subject to the same kind of forces as the gas, it should contribute in some measure to accelerate the liquid. Unlike the spherical cap bubbles, the drag coefficient for the particles is a function of the Reynolds number. The following correlation was used in this work:

$$C_{Dp} = \frac{24}{\mathrm{Re}_{pl}}(1 + 0.15\ \mathrm{Re}_{pl}^{0.687}) \qquad [21]$$

which is accurate to within 5 pct for $\mathrm{Re}_{pl} < 800$.[8] Here Re_{pl} is the particle Reynolds number in the liquid.

$$\mathrm{Re}_{pl} = \frac{\rho_l d_p (U_p - U_l)}{\mu_l} \qquad [22]$$

Figure 9 shows the effect on the average liquid velocity of changes in mass velocity of gas and powder. In this case all powder is in the liquid phase. One sees that gas flow controls the liquid velocity at high W_g or at low W_p. This would be the case in most powder injection processes where solid to gas loadings are between 2 and 200 kg solid/m^3 gas. At low W_g the powder controls the liquid velocity; this is expected to correspond to wire feeding processes where little or no gas accompanies the release of the powder. The predicted particle velocities were almost equal to the liquid velocities. The particle size used was 100 μm for which the terminal velocity was only 3.7 × 10^{-3} m per second.

For powders which are not wetted by the liquid, one may expect that a fraction of the powder travels inside the gas bubbles. This loading of the bubbles has the effect of slowing down the liquid since a denser gas exerts less force on the liquid than a light gas for the same flowrate due to lower volume concentration. This is shown in Figure 10 where the effect of varying the volume fraction of powder inside the gas (f) is compared with the gas only case.

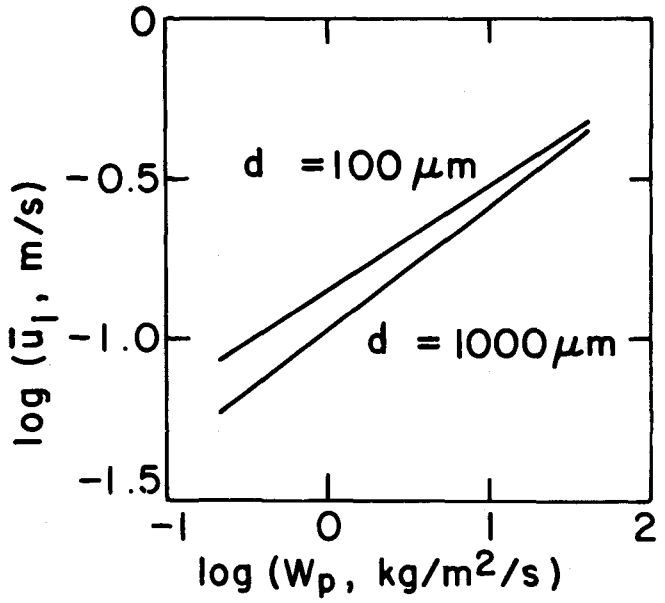

Fig. 11 — Average liquid velocity for the case of powder only for two powder sizes. CaSi-iron system, H = 1.5 m, D_L = 2.2 m.

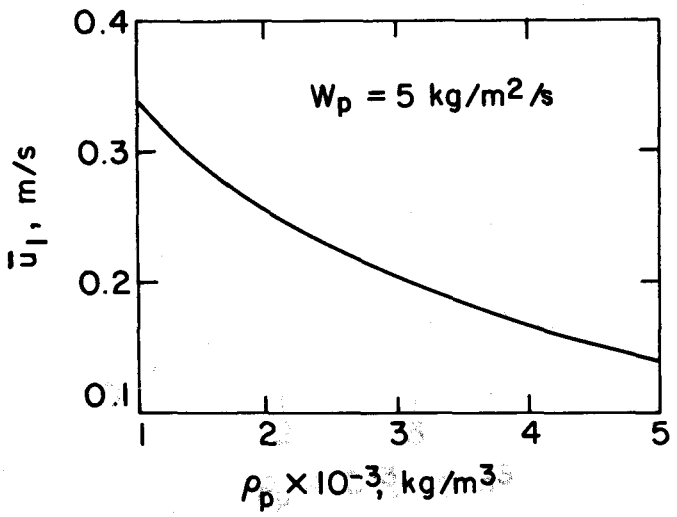

Fig. 12 — Effect of particle density on average liquid velocity. Iron is the liquid, d_p = 100 μm, H = 1.5 m, D_L = 2.2 m.

F. *Powder Only Plumes*

These are situations where the plume may consist of powder only, typically wire feeding of rare earth oxides without porous plug agitation. It is expected that in these circumstances the powder will accelerate the liquid in a similar way as gas alone does provided that the volume flow rate of powder is large. However, the wire injection rates are usually low, so that liquid velocity and recirculation rate are low. Thus many wire injection processes employ porous plug stirring to enhance mixing and inclusion removal. Figure 11 shows the case for two particle sizes. As in the case of gas, smaller particles are more effective in accelerating the liquid than large ones. Powder density is also an important variable; Figure 12 shows that, as expected, increasing particle density decreases liquid velocity. In the extreme case of equal particle and liquid density the liquid velocity is zero.

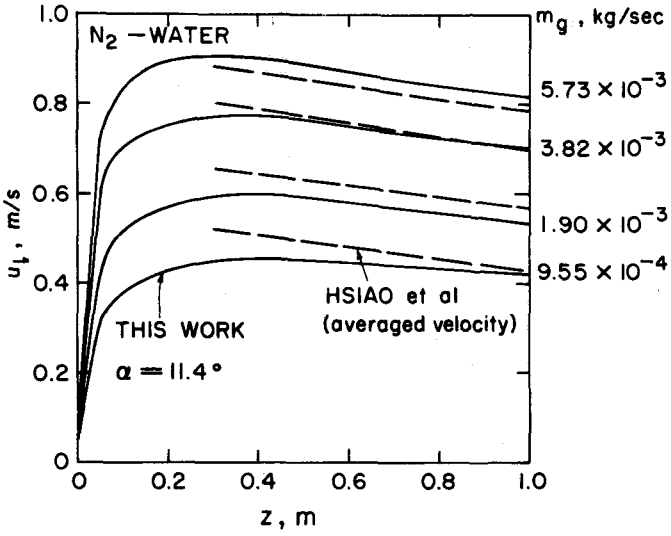

Fig. 13 — Comparison between model predictions and experimental results by Hsiao *et al.*[10] N_2-water system, D_j = 0.1 m, α = 11.4 deg, H = 1 m, D_L = 1.1 m, d_b = 0.02 m.

IV. DISCUSSION

The results of the previous section are, strictly speaking, only applicable to plumes developing from downward facing lances where conditions are clearly defined. In such cases the bubbles start out at near zero velocity and have a well-defined shape and size. The model as yet is not applicable to high velocity injection from tuyeres where there is a strong deceleration of the gas by inertial forces which has not been accounted for in the present modeling. It is thought that plumes evolving from porous elements are represented better by the model.

The experimental results of Hsiao *et al.*[10] have been examined in light of the present model. In their case the gas was introduced through a porous plug of unreported dimensions at a depth of 1 m of water. The model was run assuming that the gas had been introduced through a 10 cm diameter porous plug and that the plume expanded at an angle of 11.4 deg which was deduced from their measured velocity profiles for the $m_g = 3.82 \times 10^{-3}$ kg per second case. The bubble diameter was assumed to be 20 mm. Computed results are shown in Figure 13, which were generated for the plume geometry of the $m_g = 3.82 \times 10^{-3}$ kg per second case. Close agreement was obtained for this case, but the predicted velocities for lower flow rates were somewhat smaller, and for the higher flow rate somewhat larger. This is to be expected since the plume was probably wider at the higher injection rate, and narrower at the lower rates. No geometry information was available for all the conditions. It should be noted that the velocities reported by Hsiao *et al.* were measured at the plume axis. In Figure 11 we have plotted the average velocity based on a Gaussian radial distribution as discussed by Sahai and Guthrie.[6]

Results of this work have been compared with the work of Sahai and Guthrie[6] and Sano and Mori[4] for the N_2-iron

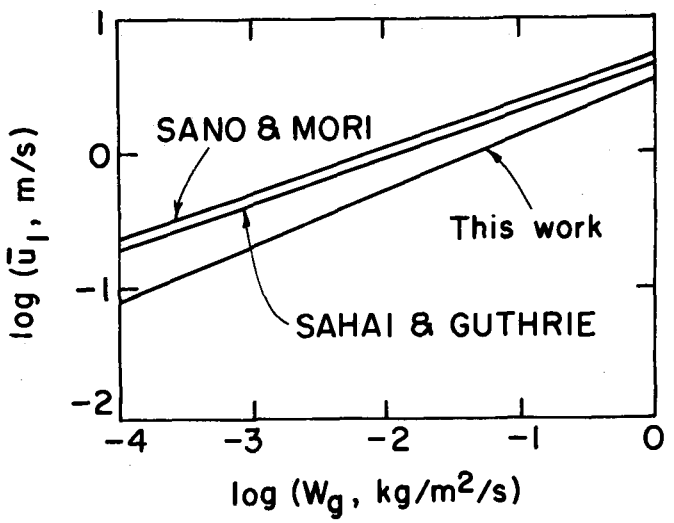

Fig. 14—Comparison between this work and other plume models N_2-iron system, $D_L = H = 3.56$ m, $d_b = 0.05$ m.

system in Figure 14. Average liquid velocity predictions by the present model are somewhat lower than the predictions by the other investigators. Closer agreement was found in the N_2-water system. It should be noted that the slope in Figure 14 is slightly higher (0.42) than that of Sahai and Guthrie (0.33) and Sano and Mori (0.346). The case of Sano and Mori and the present model are directly comparable because both assume a cylindrical plume and both have the liquid velocity as a function of the flow rate of gas per unit area of plume. In the case of Sahai and Guthrie, no mention is made of the plume geometry, and thus the comparison in Figure 14 was prepared on the basis of a cylindrical plume of 0.8 m diameter. The results of the other two models are very similar; this is because both models balance the energy input with the turbulent dissipation in the bulk liquid. Their methods for calculating the energies differ slightly.

In the present one-dimensional model, the other two dimensions are handled by assuming that the plume dimensions are determined experimentally and that the plume is axisymmetric. The model parameters are averaged evenly over the plume cross-section. It is well-known from experiment that void fraction and liquid and gas velocities vary across the plume, and are usually fitted to a Gaussian distribution. In order to develop a three-dimensional or a two-dimensional axisymmetrical differential model, one requires knowledge of the mechanism which distributes the momentum and mass across the plume. The Gaussian distribution of the void fraction suggests a diffusion type of process, and in fact bubble diffusivities have been proposed. Since this is clearly not a molecular process, the bubble diffusivity would be expected to vary with fluid properties, the intensity of turbulence, and position. Until such factors are determined, all of the two-dimensional models require the empirical input of the Gaussian distribution parameters or plume dimensions;[4,5,6] in other words the radial momentum and mass equations have not been solved. It should be noted that McKelliget *et al.*[7] employed a turbulent diffusivity for the *liquid* fraction in their mixture model. They assumed that the turbulence and mixing diffusion of liquid was the same as in a fuel/gas mixture where density differences between the phases are small and buoyancy forces may be ignored. Their model also ignored the discreteness of each phase, which, as they state, is true only if the bubbles are small in comparison with the scale of turbulence.

In the absence of any true two-dimensional model, one must assume a distribution of mass and velocity. In the present work, average ones across the cross-section of the plume have been used. It is believed that this approach will yield average velocities and temperatures useful for engineering calculations.

This model can be extended to include heat transfer and mass transfer calculations.[14] By applying heat transfer coefficients between each phase, in an analogous way to the drag coefficients, the temperatures of each phase can be calculated as they rise in the plume. Similarly, mass transfer coefficients can be applied to calculate rates of refining and other chemical reactions. These model calculations are being carried out in conjunction with high temperature measurements to ensure that appropriate heat and mass transfer coefficients are employed in these multi-phase models. It is expected that these models will quantitatively describe thermally-driven mass transfer processes such as the vaporization of magnesium and calcium or the decomposition of calcium carbonate in iron or steel and other mass transfer processes such as desulfurization and deoxidation reactions during powder and wire injection.

V. CONCLUSIONS

A one-dimensional steady-state model has been developed to describe the fluid dynamic processes in rising gas-liquid-solid plumes resulting from the injection of gas and/or solids into liquids. This appears to be the first differential model to determine gas, liquid, and solid velocities and volume fractions in such situations. The computed results agree well with available plume velocities in water. The effects of plume geometry, initial conditions, density of the phases, head of liquid, bubble size, the loading and properties of the powder are assessed. It is believed this model can be extended to include the effects of low rates of mass transfer (*e.g.*, desulfurization and other refining reactions) and high rates of mass transfer (*e.g.*, gas releasing reactions).

LIST OF SYMBOLS

A_p	area of plume (m^2)
C_D	drag coefficient (—)
d	diameter (equivalent for bubbles) (m)
D_p	plume diameter (m)
D_j	jet diameter at maximum penetration (m)
f	fraction of powder inside gas bubbles (—)
F^B_{gp}	buoyancy force on the gas-powder (in gas) mixture (N/m)
F^B_p	buoyancy force on the powder in the liquid (N/m)
F^D_{gp-l}	drag force on the gas-powder (in gas) mixture (N/m)
F^D_{p-l}	drag force on the powder in the liquid (N/m)
g	gravitational acceleration (m/s^2)
H	depth of plume (m)
m	mass flow rate (kg/s)

Q_{gm} mean gas flow rate (m^3/s)
R engineering gas constant (J/kg/K)
Re Reynolds number $\rho dU/\mu$ (—)
T temperature (K)
U velocity (m/s)
W mass velocity of a phase ($kg/m^2/s$)
Z vertical distance from bottom of plume (m)
α plume cone angle (—)
μ viscosity (kg/m/s)
ρ density (kg/m^3)
ρ_m mass of gas-powder (in gas) per unit volume of plume $\theta_g \rho_g + f \theta_p \rho_p$ (kg/m^3)
θ phase volume concentration (—)

Subscripts

atm atmospheric
b bubble
bl bulk liquid
g gas
gp particle in gas
l liquid
L ladle
m mixture
p particle, plume
pl particle in liquid
T terminal

Superscripts

o at lance tip

ACKNOWLEDGMENTS

The authors would like to express their gratitude to the American Iron and Steel Institute and the Natural Sciences and Engineering Research Council of Canada for financial support of this work.

REFERENCES

1. G. A. Irons: *ISS Transactions*, 1984, vol. 5, pp. 33-45.
2. G. A. Irons and L. R. Farias: *Metall. Trans. B*, 1985, vol. 16B, pp. 211-25.
3. G. B. Wallis: *One Dimensional Two Phase Flow*, McGraw-Hill, New York, NY, 1969.
4. M. Sano and K. Mori: *Proceedings of Scaninject III Conference*, 1983, Luleå, Sweden, June 15–17, Mefos and Jernkontoret, pp. 6:1-6:17.
5. N. El-Kaddah and J. Szekely: *Ironmaking and Steelmaking*, 1981, no. 6, pp. 269-78.
6. Y. Sahai and R. I. L. Guthrie: *Metall. Trans. B*, 1982, vol. 13B, pp. 193-202.
7. J. W. McKelliget, M. Cross, and R. D. Gibson: *Appl. Math. Modelling*, 1982, vol. 6, pp. 469-80.
8. R. Clift, J. R. Grace, and M. E. Weber: *Bubbles, Drops and Particles*, Academic Press, New York, NY, 1978.
9. C. W. Gear: *Numerical Initial Value Problems in Ordinary Differential Equations*, Prentice-Hall, Englewood Cliffs, NJ, 1971.
10. T. Hsiao, T. Lehner, and B. Kjellberg: *Scan. J. of Metall.*, 1980, vol. 9, pp. 105-10.
11. J. Szekely, T. Lehner, and C. W. Chang: *Ironmaking and Steelmaking*, 1979, no. 6, pp. 285-93.
12. R. J. Fruehan and L. J. Martonik: *3rd Iron and Steel Congress*, Chicago, IL, 1978, pp. 229-38.
13. M. Sano and K. Mori: *Transactions ISIJ*, 1980, vol. 20, pp. 675-81.
14. G. A. Irons, L. R. Farias, and L. K. Chiang: unpublished research, McMaster University, Hamilton, ON, Canada, 1985.